Disease Models & Mechanisms 1, 155-167 (2008) doi:10.1242/dmm.000596

Visualizing stromal cell dynamics in different tumor microenvironments by spinning disk confocal microscopy

Mikala Egeblad[1,*,‡], Andrew J. Ewald[1,‡], Hanne A. Askautrud[1,2], Morgan L. Truitt[1], Bryan E. Welm[1,5], Emma Bainbridge[1], George Peeters[3], Matthew F. Krummel[4] and Zena Werb[1,*]

SUMMARY

The tumor microenvironment consists of stromal cells and extracellular factors that evolve in parallel with carcinoma cells. To gain insights into the activities of stromal cell populations, we developed and applied multicolor imaging techniques to analyze the behavior of these cells within different tumor microenvironments in the same live mouse. We found that regulatory T-lymphocytes (Tregs) migrated in proximity to blood vessels. Dendritic-like cells, myeloid cells and carcinoma-associated fibroblasts all exhibited higher motility in the microenvironment at the tumor periphery than within the tumor mass. Since oxygen levels differ between tumor microenvironments, we tested if acute hypoxia could account for the differences in cell migration. Direct visualization revealed that Tregs ceased migration under acute systemic hypoxia, whereas myeloid cells continued migrating. In the same mouse and microenvironment, we experimentally subdivided the myeloid cell population and revealed that uptake of fluorescent dextran defined a low-motility subpopulation expressing markers of tumor-promoting, alternatively activated macrophages. In contrast, fluorescent anti-Gr1 antibodies marked myeloid cells patrolling inside tumor vessels and in the stroma. Our techniques allow real-time combinatorial analysis of cell populations based on spatial location, gene expression, behavior and cell surface molecules within intact tumors. The techniques are not limited to investigations in cancer, but could give new insights into cell behavior more broadly in development and disease.

INTRODUCTION

Solid tumors contain many different cellular components in addition to tumor cells, including fibroblasts, lymphocytes, dendritic cells, macrophages and other myeloid cells. The tumor microenvironment is defined by these stromal cells, as well as extracellular matrix components (e.g. collagens and fibronectins), growth factors, proteases and even oxygen and metabolites. The composition of the microenvironment varies with tumor stage, and influences both cancer cell and stromal cell functions. Changes in the stromal compartment that occur with increasing tumor stage include alteration of the function of vascular cells and tumor-associated fibroblasts, and increasing influx of inflammatory cells (Bissell and Radisky, 2001; Coussens and Werb, 2002; Lewis and Pollard, 2006).

The different stromal cell types have distinct functions in cancer progression: myeloid cells and fibroblasts can accelerate tumor progression through the recruitment of new vasculature, and through secretion of chemokines, matrix metalloproteinases and growth factors (Egeblad and Werb, 2002; Bhowmick and Moses, 2005; Lewis and Pollard, 2006; Du et al., 2008); dendritic cells can present tumor antigens to activate an anti-tumor immune response (Banchereau and Palucka, 2005); and T-regulatory lymphocytes (Tregs) can downregulate the activity of cytotoxic T-lymphocytes against cancer cells (Colombo and Piconese, 2007). These tumor-associated stromal cells are distinct from their counterparts in normal tissue and are probably heterogeneous in function (Sica and Bronte, 2007).

Pioneering studies have established intravital imaging techniques for analyzing cell dynamics within the tissues of live mice, including within tumors (Brown et al., 2001; Jain et al., 2002; Brown et al., 2003; Halin et al., 2005; Hoffman, 2005; Stroh et al., 2005; Dreher et al., 2006; Sidani et al., 2006; Boissonnas et al., 2007). However, intravital imaging of tumors has been limited by difficulties in contrasting the dynamics of multiple cell types in different tumor microenvironments for extended time periods.

Building on previous efforts, we sought to compare the dynamics of stromal cells between different tumor microenvironments by direct observation. This goal presented several key challenges: (a) the ability to analyze different tumor microenvironments within the same mouse, thereby excluding mouse-to-mouse variation, (b) labeling of different tumor components, (c) a multicolor excitation and detection scheme to follow multiple cell types, (d) optical access to tumors, (e) long-term anesthesia, and finally, (f) fast image collection to minimize motion artifacts. To achieve this goal, we developed and refined a suite of techniques enabling four-color, multi-position, dynamic imaging for extended time periods in different tumor microenvironments within the same live mouse. The application of these techniques has given us new insights into the tumor microenvironment by allowing us to contrast stromal cell behavior between microenvironments. Furthermore, the techniques enabled the subdivision of myeloid cells into distinct subpopulations in vivo, based on their endocytic and migratory

[1]Department of Anatomy and [4]Department of Pathology, University of California, San Francisco, 513 Parnassus Avenue, San Francisco, CA 94143, USA
[2]Department of Medical Genetics, Ullevål University Hospital and Faculty of Medicine, University of Oslo, Boks 1072 Blindern, NO-0316 Oslo, Norway
[3]Solamere Technology Group, 1427 Perry Avenue, Salt Lake City, UT 84103, USA
[5]Present address: Department of Surgery, Huntsman Cancer Institute, University of Utah, 2000 Circle of Hope, Salt Lake City, UT 84112, USA
*Authors for correspondence (e-mail: mikala.egeblad@ucsf.edu; zena.werb@ucsf.edu)
‡These authors contributed equally to this work

behavior, and their expression of surface markers. Our techniques, together with the use of model organisms, provide a versatile platform for examining the contribution of cell behavior to a range of diseases, including cancer, and infectious and cardiovascular diseases.

RESULTS

Design of a four-color, multi-region, time-lapse, micro-lensed, spinning disk confocal microscope to investigate tumor microenvironments in live mice

To study stromal cell dynamics by live imaging, we developed a suite of techniques: we designed our microscope around a spinning disk confocal scan-head and a high-sensitivity, intensified charge-coupled device (ICCD) camera (supplementary material Fig. S1). This achieved image acquisition times of 17 and 33 milliseconds for 512×512 and 1024×1024 pixel images, respectively. We used a robotic stage to allow multi-position, sequential imaging in different tissue microenvironments within the same mouse. Since enhanced cyan fluorescent protein (ECFP) or enhanced green fluorescent protein (EGFP) are most commonly used in reporter mouse lines, we accommodated simultaneous imaging of ECFP and EGFP using excitation selectivity of 405 and 488 nm light, and added 568 and 647 nm excitation for four-color imaging (supplementary material Fig. S2). Within a 12-hour experiment, we typically collected 32,400 images (540 exposures for each of the four colors in three z-planes in five fields). Accordingly, minimizing the moving parts was essential and was achieved using electronic control of the 405 nm solid-state laser, an acousto-optic tunable filter for the argon and krypton lasers, a quadruple pass dichroic and a corresponding excitation clean-up filter.

We gained optical access to the mouse mammary gland by creating a skin flap. Careful monitoring of vital signs and oximetry, and maintenance of normothermia and hydration facilitated mouse anesthesia for a median duration of 7 hours 29 minutes (range: 2 hours 46 minutes-27 hours 29 minutes; *n*=69 mice). It was feasible to image up to 70 μm into the tissue from the first detectable cell layer (supplementary material Fig. S3). Photobleaching of commonly used fluorescent proteins was negligible, as tested by imaging a single field in two colors, 1000 times (supplementary material Fig. S3). Imaging was possible in a well-lit room, aiding monitoring of the live mouse.

Differential behavior of inflammatory cell populations in different tumor microenvironments

Tumor-infiltrating leukocytes include lymphocytes, dendritic cells, myeloid-derived suppressor cells (MDSCs) and macrophages – each cell type having different functions. To investigate the dynamics of tumor-infiltrating leukocytes, we used the *MMTV-PyMT* mouse model of mammary carcinoma. This model is progressive (Fig. 1A), with different tumor stages present within the same mammary gland (Lin et al., 2003), and exhibits leukocyte infiltration at all stages (Fig. 1B; supplementary material Fig. S4). We labeled stromal cells through cross-breeding with different mouse lines that each expressed EGFP in different cell populations and at different intensities (Fig. 1D,E,F; Fig. 5). For contrast, we crossbred these mice with the *ACTB-ECFP* line to label all cells with ECFP, although the labeling was strongest in the epithelial compartment (Fig. 1C).

Tumor-infiltrating Tregs can downregulate the tumoricidal immune response (Colombo and Piconese, 2007); however, it is not known how the cells behave in intact tumors. We imaged Tregs expressing a fusion-protein of EGFP and the transcription factor Foxp3 (preferentially expressed in Tregs), by crossing *MMTV-PyMT;ACTB-ECFP* mice with the *Foxp3*^{EGFP} mouse line (Fontenot et al., 2005) (Fig. 1D). Most Tregs were migratory; 55% migrated with an average track length/time of 8 μm/minute (range: 1-14 μm/minute; *n*=130 cells from three mice) and an average displacement of 3 μm/minute (range: 0.3-11 μm/minute; *n*=130 cells from three mice). An additional 14% of the Tregs migrated, but stopped for short intervals (average: 18 minutes; range: 8-46 minutes), typically migrating along, or in proximity to, blood vessels. The median of the furthest distance between a moving Treg and a blood vessel was 20 μm (range: 0-100 μm; *n*=98 cells from five mice), whereas the median of the shortest distance was 5 μm (range: 0-90 μm; *n*=98 cells from five mice; supplementary material Movie 1). Few Tregs infiltrated the tumor mass and of those that did, none migrated. The average velocity and proportions of migrating Tregs, their arrest times and their tendency to migrate along blood vessels were similar to previous reports on tumor-infiltrating cytotoxic T-lymphocytes (Mrass et al., 2006; Boissonnas et al., 2007).

Tumor-infiltrating antigen-presenting cells, including CD11c$^+$ dendritic cells, have the potential of enhancing the immune response to solid tumors (Labeur et al., 1999). We imaged CD11c$^+$ dendritic-like cells expressing a membrane-targeted fusion-protein of EGFP with the diphtheria toxin receptor (DTR; allowing us to observe the membrane extensions as the cells moved through the tissue) by crossing *MMTV-PyMT;ACTB-ECFP* mice with the *CD11c-DTR-EGFP* mouse line (Fig. 1E; supplementary material Movie 2). Most dendritic-like cells were migratory, typically at the tumor-stroma border (supplementary material Movies 2,3), although they occasionally stopped and formed longer interactions with cancer cells (supplementary material Movie 2). Dendritic-like cells more commonly infiltrated the tumor mass than Tregs, but those that did were also non-migratory (supplementary material Movie 3). The ability to image CD11c$^+$ dendritic-like cells using spinning disk confocal imaging additionally served as a proof-of-principle that our microscope could detect EGFP-levels barely above the detection limits of fluorescence-activated cell sorting (FACS) (Fig. 1G,H).

Myeloid cells are the most abundant and heterogeneous class of cells that infiltrate tumors (supplementary material Fig. S4). Tumor-promoting myeloid cells fall into two broad groups, the MDSCs and the tumor-associated macrophages (TAMs), and their increased abundance correlates with poor prognosis (Sica and Bronte, 2007). Since the tumor microenvironment may directly influence cell function (Bissell and Radisky, 2001; Lewis and Pollard, 2006), we hypothesized that this would be reflected in observable differences in myeloid cell behavior between microenvironments. To test this hypothesis, we compared the behavior of myeloid cells in normal mammary glands, premalignant hyperplasias and in different areas of carcinomas, by crossing *MMTV-PyMT;ACTB-ECFP* mice with the *c-fms-EGFP* mouse line, which expresses EGFP under the c-fms promoter (Fig. 2A,A′; supplementary material Movies 4,5). Myeloid cells positive for c-fms were markedly more migratory in the tumor-stroma border

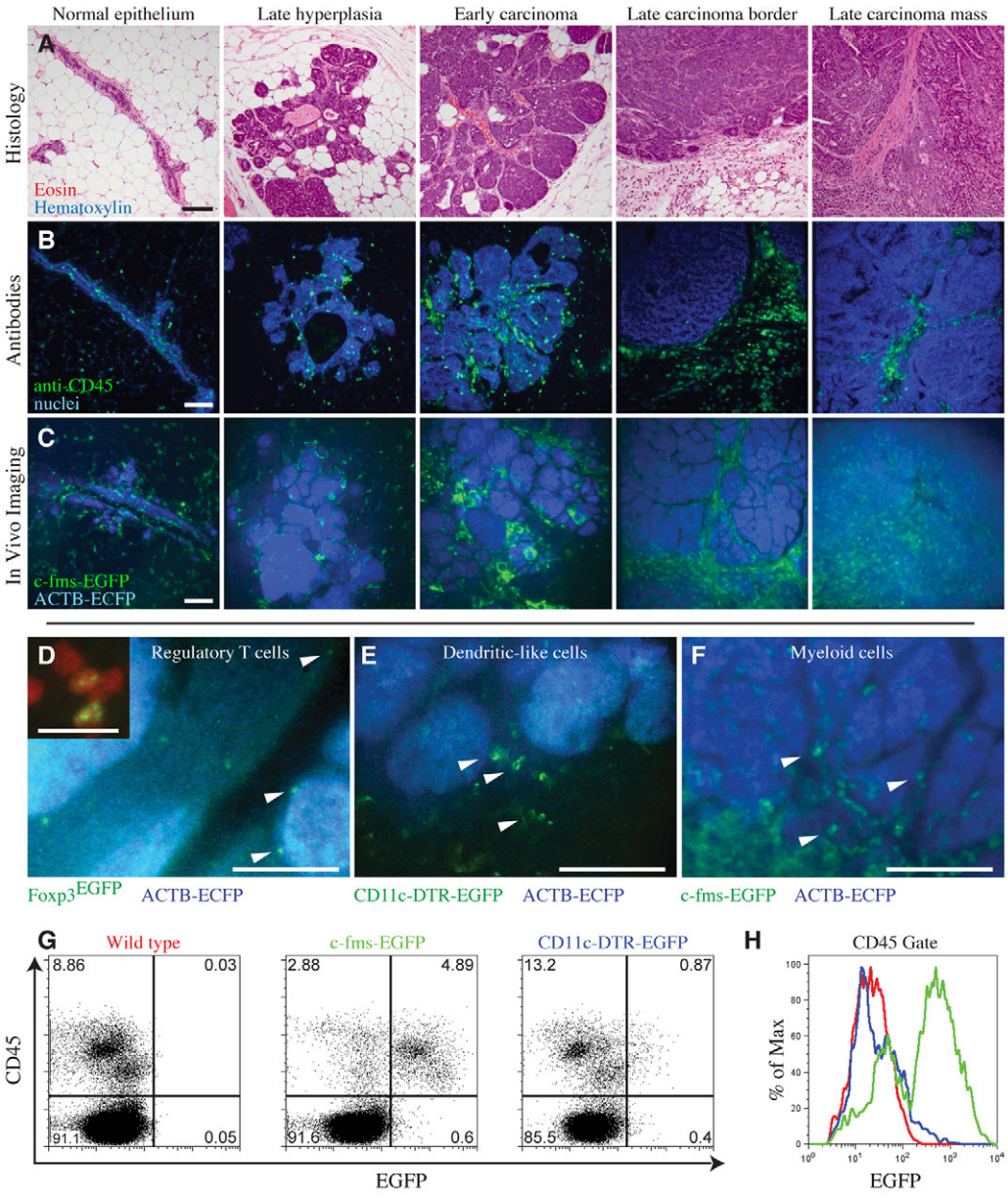

Fig. 1. Leukocyte imaging in MMTV-PyMT mammary carcinoma.
(A) Examples of stages of MMTV-PyMT tumors are shown together with a normal duct from a wild-type mouse (hematoxylin and eosin stained sections). (B) Leukocytes (anti-CD45, green) in mammary tissue and MMTV-PyMT tumors (nuclei stained with propidium iodide and colored blue). (C) Different tumor microenvironments within live *MMTV-PyMT;ACTB-ECFP;c-fms-EGFP* mice. The normal duct is from a live *ACTB-ECFP;c-fms-EGFP* mouse. Myeloid cells are green (c-fms-EGFP) and all cells are labeled blue (ACTB-ECFP). (D) Nuclear EGFP (white arrowheads) in Foxp3^{+} Tregs in a tumor within a live *MMTV-PyMT;ACTB-ECFP;Foxp3^{EGFP}* mouse. Insert shows colocalization of green EGFP nuclear staining with DNA (propidium iodide, red) in lymph node cells (frozen section). (See supplementary material Movie 1.) (E) Membrane EGFP (white arrowheads) in CD11c^{+} dendritic-like cells in a tumor within a live *MMTV-PyMT;ACTB-ECFP;CD11-DTR-EGFP* mouse. (See supplementary material Movie 2.) (F) Cytoplasmic EGFP (white arrowheads) expressed in c-fms^{+} myeloid cells in a tumor within a live *MMTV-PyMT;ACTB-ECFP;c-fms-EGFP* mouse. (See supplementary material Movie 5.) (G) Comparison of the EGFP intensity of infiltrating leukocytes isolated from mammary glands of *c-fms-EGFP* and *CD11c-DTR-EGFP* mice. The percentages of cells are indicated in each quadrant. (H) Intensity in the EGFP channel of leukocytes isolated from mammary glands of wild-type (red), *c-fms-EGFP* (green) and *CD11c-DTR-EGFP* (blue) mice, gated on CD45^{+} cells and all collected with the same settings. Images in C-F are maximum intensity projections. Bars, 100 μm.

areas than within the tumor mass, regardless of tumor stage (supplementary material Movie 5). We computed trajectories of individual myeloid cells within different areas, to determine the average displacement over time (Fig. 2A′). In accordance with previous studies (Lindquist et al., 2004), we found that cells with a computed displacement of less than 2 μm/minutes were virtually non-migratory when observed directly, and that their pseudo-migration was a result of motion artifacts. The tumor-stroma border areas of carcinomas contained the highest fractions of cells with medium (2-4 μm/minute) and fast (>4 μm/minute) displacement/time. The lowest fractions of medium and fast migrating cells were found inside the tumor mass at the carcinoma stage (Table 1, P<0.0001, chi-squared test). Thus, using multi-position imaging, we found that the myeloid cell population displays heterogeneity, with cell migration varying between tumor microenvironments in the same mouse.

Differential response of cell migration to acute hypoxia

Next, we asked whether oxygen tension, a microenvironmental factor, could be responsible for the observed differences in cell migration between microenvironments; for example, lymphocyte migration in explanted lymph nodes is very sensitive to oxygen concentration (Huang et al., 2007). Since oxygen tension varies widely between different parts of tumors (Brown and Wilson, 2004), we hypothesized that differences in myeloid cell migration between microenvironments, in part, represented differences in tissue oxygen tension. We induced acute systemic hypoxia by lowering inhaled oxygen levels from 21% to 7%, but this did not reduce myeloid cell migration acutely (Fig. 2B). In contrast, most Tregs stopped migrating almost immediately upon acute systemic hypoxia (Fig. 2C; supplementary material Movie 6). Interestingly, the Tregs resumed migration when normoxia was re-established (Fig. 2C; supplementary material Movie 6).

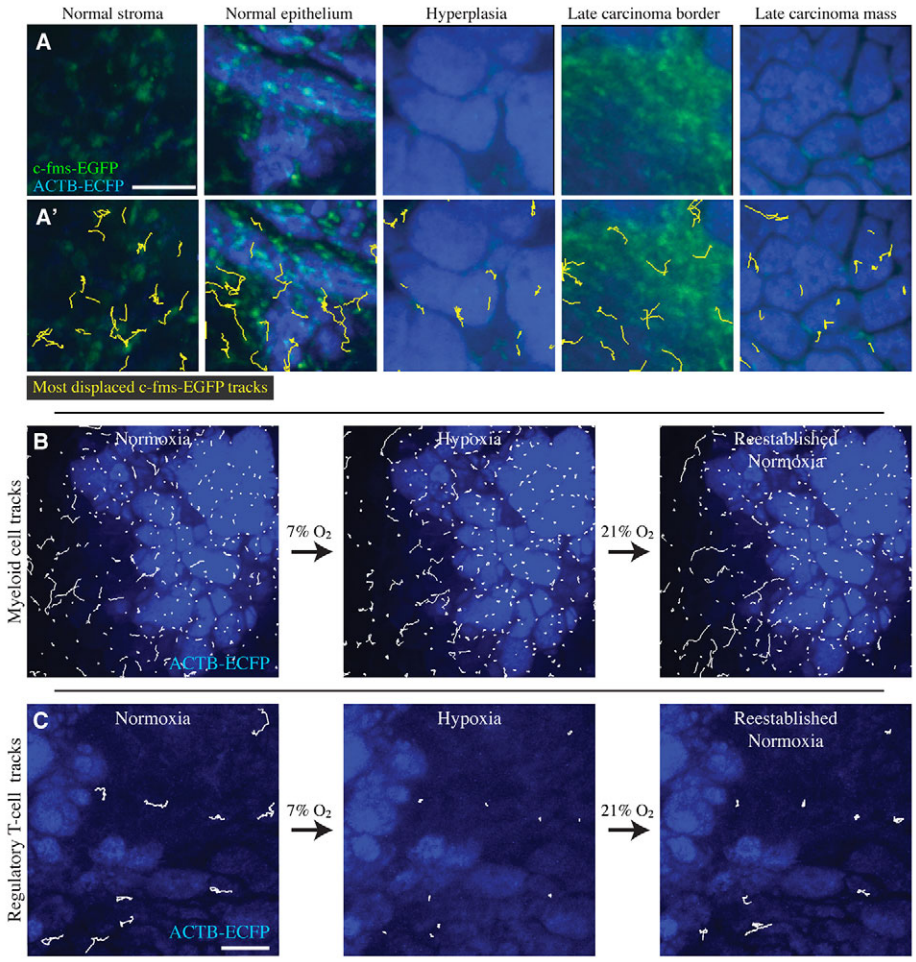

Fig. 2. Myeloid cell behavior within different tumor microenvironments in MMTV-PyMT tumors. (A) Different microenvironments from normal mammary glands and mammary carcinomas with (A') the twenty most displaced trajectories of single c-fms$^+$ myeloid cells tracked over 1 hour. The fields from the normal mammary gland are sequentially imaged from the same mouse, and all the fields from mammary carcinomas are sequentially imaged from another mouse (maximum intensity projections). (See supplementary material Movies 4,5.) (B) c-fms$^+$ myeloid cells do not respond to acute systemic hypoxia. c-fms+ cells were tracked during 20 minutes of normoxia (21% inhaled oxygen), 20 minutes of acute systemic hypoxia (7% inhaled oxygen) and 20 minutes of re-established normoxia in the same field. Images are representative of three mice. (C) Foxp3$^+$ Tregs cease migration following acute systemic hypoxia in a live *MMTV-PyMT;ACTB-ECFP;Foxp3^{EGFP}* mouse. The same ten cells were tracked during 20 minutes of normoxia (21% inhaled oxygen), 20 minutes of systemic acute hypoxia (7% inhaled oxygen) and 20 minutes of re-established normoxia in the same field. Images are representative of four mice. (See supplementary material Movie 6.) Bars, 100 μm.

Dextran uptake up by a low-migratory, mannose receptor$^+$ macrophage population

Since acute changes in oxygen levels did not influence myeloid cell migration, we determined whether the distinctive behaviors of the myeloid cells in the different microenvironments represented different myeloid cell types (e.g. monocytes, macrophages, granulocytes, dendritic cells and MDSCs). Essentially all c-fms-EGFP-positive cells expressed CD11b (Fig. 3A). Several different subsets of myeloid cells could be recognized in late stage tumors – 68% expressed both CD11b and the macrophage marker F4/80, whereas 47% expressed both CD11b and CD11c [a dendritic cell marker also expressed by some macrophages (Grundy and Sentman, 2005)]. In addition, 13% co-expressed CD11b and Gr1 (Ly-6G), a marker for neutrophils and MDSCs (Mordue and Sibley, 2003; Gabrilovich et al., 2007) (Fig. 3A).

To analyze the behavior of different subsets of c-fms$^+$ myeloid cells within the same mouse and microenvironment simultaneously, we first marked the macrophages with intravenously injected fluorescent dextran (Wyckoff et al., 2007), which over time leaked out of tumor areas and was taken up by a subset of c-fms$^+$ myeloid cells. In the tumor periphery, dextran-ingesting c-fms$^+$ macrophages were non-migratory by direct inspection, even before ingesting dextran, whereas myeloid cells that did not ingest dextran were migratory in these same areas (Fig. 3B; supplementary material Movie 7). We computed trajectories of the total c-fms$^+$ myeloid cell population, as well as from the dextran-ingesting cell

Table 1. Migratory behavior of myeloid cells varies with the tumor microenvironment

	Normal			Late carcinoma	
Velocity	**Stroma (*n*=385)**	**Epithelium (*n*=980)**	**Hyperplasia (*n*=1093)**	**Border (*n*=1724)**	**Tumor mass (*n*=816)**
Slow: <2 μm/minute	91%	87%	92%	81%	93%
Medium: 2-4 μm/minute	8%	12%	7%	15%	6%
Fast: >2 μm/minute	1%	1%	1%	3%	1%

Velocity of c-fms$^+$ cells were computed from four 1-hour-long time-lapse movies of 200x200 μm fields per microenvironment. Fields with normal epithelium and hyperplasia also contained some of the adjacent stroma. The distribution of myeloid cell velocities differed significantly between the microenvironments (P<0.0001, chi-squared test).

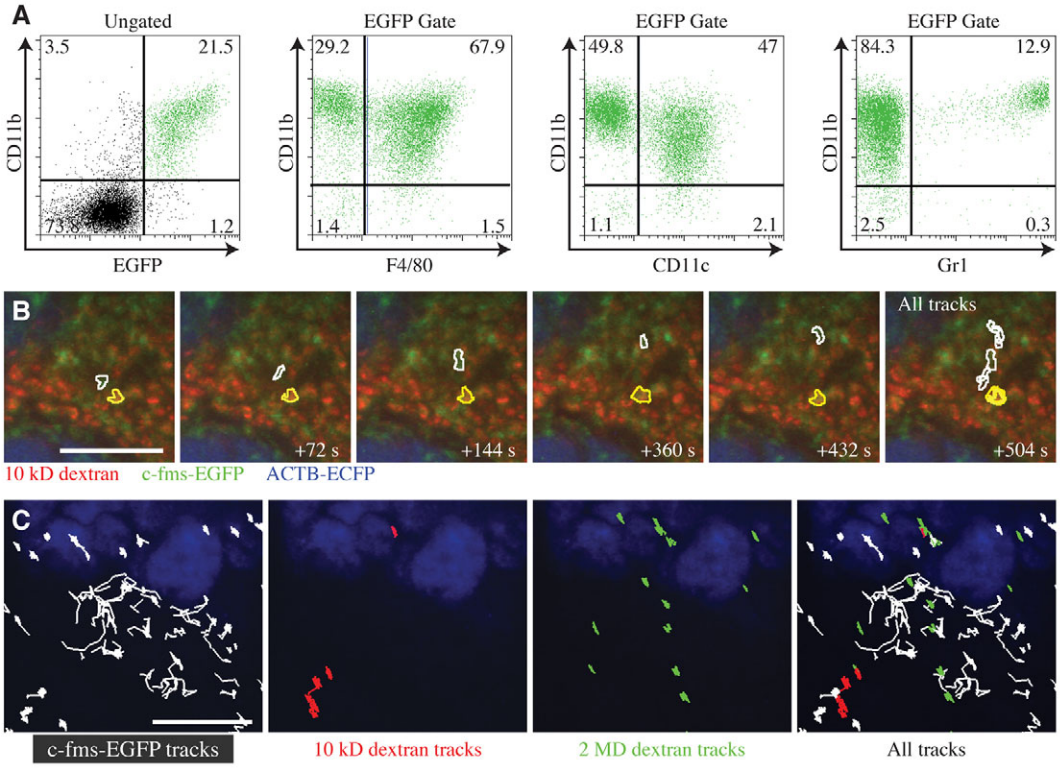

Fig. 3. Migratory behavior of subpopulations of myeloid cells in MMTV-PyMT carcinoma. (A) The majority of c-fms-EGFP$^+$ cells in late carcinomas of *MMTV-PyMT;c-fms-EGFP* tumors are myeloid cells (positive for CD11b when analyzing all single cells isolated from tumors by FACS, ungated). Most of the c-fms-EGFP$^+$ cells are double positive for CD11b and F4/80 markers (macrophage-like), whereas fewer are double positive for CD11b and CD11c (dendritic-like) or CD11b and Gr1 (neutrophils and MDSCs). The percentages of cells are indicated in each quadrant. (B) Example of migration of two myeloid cells at the border of a late carcinoma – a low-migratory, dextran-ingesting cell (yellow outline) and a high-migratory, dextran-negative cell (white outline). See supplementary material Movie 7 for time-lapse recordings of the same field. (C) Trajectories were computed for c-fms-EGFP$^+$ myeloid cells (white); cells that had ingested 10 kDa dextran (red) or 2 MDa dextran (green). Images are representative of six mice. See Table 2. Bars, 100 µm.

populations using both low (10 kDa) and high (2 MDa) molecular weight dextran (Fig. 3C). Although 19% of the total c-fms$^+$ myeloid cells migrated with a velocity of >2 µm/minute, only 5-6% of the dextran-ingesting macrophages migrated in the same tumor-stroma border areas (Table 2, P<0.0001, chi-squared test).

Tumor-infiltrating macrophages can be classified as either the tumoricidal, classical activated/M1 type, or as the pro-tumorigenic, alternatively activated/M2 type, which can stimulate cancer cell proliferation and invasion as well as tumor angiogenesis (Sica and Bronte, 2007). To characterize the macrophages that were marked by dextran, we isolated tumor tissue from dextran-injected mice and stained it for macrophage markers. The c-fms$^+$/dextran$^+$ cells in the tumor-stroma border areas expressed both CD68, a marker of monocytes/macrophages, and CD206 (the mannose receptor), a marker of alternatively activated M2-type macrophages (Mantovani et al., 2002) (Fig. 4A,B). The c-fms$^+$/dextran$^-$ myeloid cells in tumor-stroma border areas were mostly CD68$^+$, but negative for CD206 (Fig. 4A,B). Similarly, the c-fms$^+$/dextran$^-$ myeloid cells that had infiltrated the tumor mass (largely sessile) were CD68$^+$, but negative for CD206 (Fig. 4A′B′).

Analysis of dextran uptake to distinguish non-migratory Fsp1$^+$ macrophages from fibroblasts

To expand our analysis of the cells within the tumor microenvironment, we looked beyond leukocytes and analyzed the behavior of carcinoma-associated fibroblasts (CAFs) (Fig. 5). Since no single marker exists for CAFs, we used mice that express EGFP, under the fibroblast-specific protein 1 promoter (*Fsp1*$^{+/+.EGFP}$

Table 2. Migratory behavior varies with dextran ingestion

Velocity	c-fms$^+$ cells (n=1807)	10 kDa dextran-ingesting cells (n=1207)	2 MDa dextran-ingesting cells (n=127)
Slow: <2 µm/minute	81%	95%	94%
Medium: 2-4 µm/minute	15%	5%	5%
Fast: >2 µm/minute	3%	0%	1%

Velocity of c-fms$^+$, and 10 kDa and 2 MDa dextran-ingesting cells were computed from five fields of tumor-stroma border areas (hyperplasia, early and late carcinomas) in 1-hour-long time-lapse movies. The distribution of cell velocities differed significantly between the cell types (P<0.0001, chi-squared test).

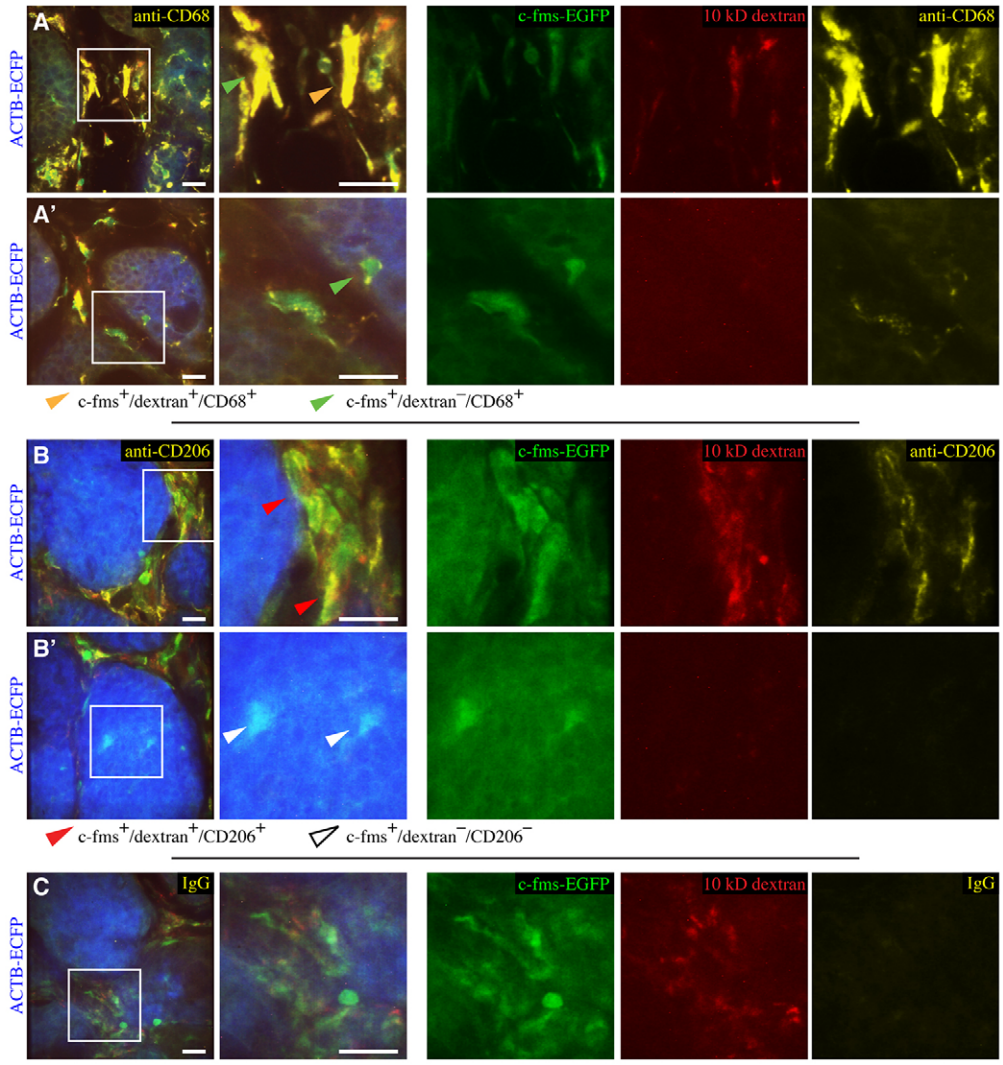

Fig. 4. Extravasated dextran is ingested by myeloid cells that express markers for alternatively activated macrophages, CD68 and CD206. (A) Myeloid cells (c-fms-EGFP, green) in the tumor-stroma border that have ingested 10 kDa dextran (red) were CD68$^+$ (yellow), a monocyte/macrophage marker, and (B) CD206$^+$, a marker of alternatively activated (M2) macrophages (yellow). (A′) Myeloid cells that had infiltrated into the tumor mass (ACTB-ECFP, blue) had not ingested dextran, were positive for CD68, (B′) but not CD206. The orange arrowhead points to a c-fms-EGFP$^+$ cell in the stroma that was CD68$^+$ and had ingested dextran; green arrowheads point to c-fms$^+$/CD68$^+$ cells in the stroma and tumor mass that had not ingested dextran; white arrowheads point to c-fms-EGFP$^+$ cells that were CD206$^-$ and had not ingested dextran; red arrowheads point to c-fms-EGFP$^+$ cells that had ingested dextran and were CD206$^+$. (C) Minimal staining was found using control IgG. Four-color overlay are shown in the first column at low magnification. The white outlined areas are shown to the right, at higher magnification, in four-color overlays and as single channels. Images are representative of five tumors. Bars, 20 μm.

mice), in both fibroblasts and macrophages (Inoue et al., 2005), and distinguished between these cell types by the propensity of macrophages to take up injected fluorescent dextran (Wyckoff et al., 2007). We imaged the fibroblasts in the stroma (Fig. 5A), at the tumor border (Fig. 5B) and within the tumor mass (Fig. 5C) from the time of dextran injection and continued imaging for several hours after the injection (supplementary material Movie 8). A small subset of Fsp1$^+$/dextran$^-$ cells (enriched for fibroblasts) was migratory, but most cells were non-migratory, regardless of whether they were interspersed in the stroma between fat cells, at the periphery of the carcinoma, or within the carcinoma mass (compare Fig. 5A-C with A′-C′; supplementary material Movie 8). Fsp1$^+$/dextran$^+$ cells (macrophages) were non-migratory.

Patrolling of blood vessels and the tumor-stroma border area by Gr1$^+$ myeloid cells

The numbers of both MDSCs (CD11b$^+$/Gr1$^+$ or c-fms$^+$/Gr1$^+$) and TAMs (c-fms$^+$/CD68$^+$) increase with tumor progression (Sica and Bronte, 2007). To analyze the behavior of different subsets of c-fms$^+$ myeloid cells, simultaneously within the same mouse and microenvironment, we labeled two myeloid cell subsets and observed them for over 12 hours. Gr1$^+$ myeloid cells (monocytes, granulocytes and MDSCs) were marked with intravenously injected fluorescent anti-Gr1 antibodies (Chiang et al., 2007), whereas alternatively activated macrophages were marked with intravenously injected fluorescent dextran (Fig. 6A,A′). Within minutes of injecting Alexa Fluor 647-conjugated anti-Gr1 antibodies together with fluorescent dextran, c-fms$^+$ cells with high levels of bound anti-Gr1 antibodies were observed patrolling inside blood vessels, both with and against the blood flow (Fig. 6A′,C; supplementary material Movie 9).

We also observed Gr1$^+$ cells extravasating into the tumor stroma (Fig. 6B), and migrating c-fms$^+$/Gr1$^+$cells at the tumor-stroma border (Fig. 6C) – although these were not as abundant as migrating c-fms$^+$/Gr1$^-$ cells. A fluorescently labeled isotype-matched control antibody was injected to control for non-specific antibody uptake or binding by the myeloid cells, but did not label cells in the tumors (supplementary material Fig. S5). The majority of the cells that ingested dextran were c-fms$^+$/Gr1$^-$ and sessile. Interestingly, there were also a few non-migratory, c-fms$^+$/Gr1$^+$/dextran$^+$ cells in the stroma, localized at the tumor-stroma border and along blood vessels (Fig. 6D). Gr1$^+$ cells were not observed inside the tumor

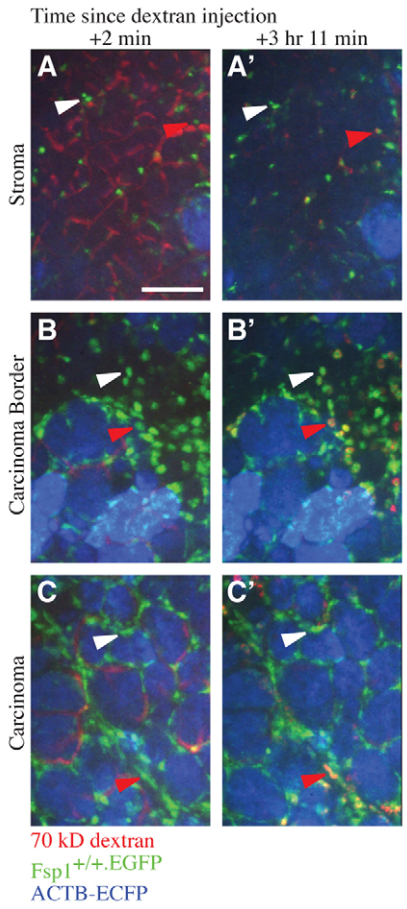

Fig. 5. Differentiation between Fsp1$^+$ fibroblasts and macrophages in a tumor within a live *MMTV-PyMT* mouse. Three fields with different tumor microenvironments, (A) stroma, (B) carcinoma border and (C) within the carcinoma, imaged in the same mouse are shown at the indicated times after dextran injection. A subset of Fsp1$^+$ cells took up injected fluorescent dextran (red arrowheads); these cells were probably macrophages. Fsp1$^+$/dextran$^-$ cells (white arrows) are enriched for fibroblasts. Images are maximum intensity projections. (See supplementary material Movie 8.)

mass during observation periods of >12 hours. Taken together, these data indicate that MDSC-like cells and TAM-like cells consist of distinct subpopulations that can be distinguished, in situ, in live mice by a combination of transgenic and cell surface markers, tissue location, and cell behavior.

DISCUSSION

The tumor microenvironment evolves with, and influences, tumor progression (Bissell and Radisky, 2001; Coussens and Werb, 2002; Lewis and Pollard, 2006). In this study, we have used long-term spinning disk confocal microscopy to perform a dynamic analysis of the varying stromal cell behavior within the evolving tumor microenvironment, analyzing Tregs, CAFs, macrophages, dendritic-like cells and myeloid cells. Furthermore, we have achieved in situ subdivision of myeloid cells into distinct populations using combinatorial labeling of cells and analysis of location, motility and endocytic behavior (Fig. 6E).

Dynamics of tumor-associated stromal cells in different microenvironments

We showed that tumor-associated stromal cells, including Foxp3$^+$ Tregs, CD11c$^+$ dendritic-like cells, c-fms$^+$ myeloid cells and Fsp1$^+$ fibroblasts, have distinct behaviors. Understanding how these cells behave in tumors may be important for understanding their roles in tumor immunology: Tregs downregulate the activity of cytotoxic T-lymphocytes against cancer cells (Colombo and Piconese, 2007); dendritic cells are used with tumor vaccines (Banchereau and Palucka, 2005); and myeloid cells accelerate tumor progression in mice and are associated with poor prognosis in human breast cancer (Condeelis and Pollard, 2006; de Visser et al., 2006; Lewis and Pollard, 2006). Interestingly, all of the analyzed stromal cell types showed a higher propensity to migrate in the peri-tumor area and lower propensity to migrate within the tumor mass. Possible explanations for the difference in cell migration could be, simply, that the cancer cells within the tumor mass are too tightly attached to each other to enable the further migration of stromal cells. Alternatively, it could be the result of either changes in chemokine concentrations, the presence of factors secreted by the cancer cells to inhibit migration, or the lack of oxygen and metabolites.

In explanted lymph nodes, T lymphocyte migration is very sensitive to changes in oxygen concentrations (Huang et al., 2007). We show that Treg migration in intact peripheral tissue within live mice is sensitive to inhaled oxygen levels. Thus, the sensitivity of lymphocyte migration to oxygen levels is unlikely to be specific to explanted lymph nodes and may explain why these cells often migrate in proximity to blood vessels. Interestingly, the cessation of migration during acute hypoxia was reversible and most Tregs resumed migration after re-establishment of systemic normoxia.

In contrast to Tregs, the myeloid cells showed little sensitivity to induction of acute systemic hypoxia. This was somewhat surprising, since it has been shown that hypoxia inhibits macrophage chemotaxis in transwell migration assays in vitro (Turner et al., 1999; Grimshaw and Balkwill, 2001). However, our observation is consistent with the ability of myeloid cells to infiltrate hypoxic areas in tumors or dermal wounds, where a more chronic exposure to hypoxia may change the ability of the cells to further migrate (Murdoch et al., 2004). The mechanism that makes lymphocyte migration sensitive to hypoxia is unknown, but lymphocytes could have sensors for oxygen or oxygen metabolites [e.g. nitric oxide (NO)], as reported for neurons in *Caenorhabditis elegans* (Gray et al., 2004). Alternatively, oxygen-dependent metabolism might be essential for migration of lymphocytes but not myeloid cells. The difference in migratory response to acute systemic hypoxia between lymphocytes and myeloid cells raises the possibility that microenvironmental differences in oxygen concentration influence tumor immunology by biasing infiltration of different immune cell populations into regions of tumors with low oxygen levels.

Molecular and cell behavioral subdivision of myeloid cells in intact tumors

Macrophages, which are of the myeloid lineage, have been proposed to respond to different tumor microenvironments by assuming distinct functions (Mantovani et al., 2002; Pollard, 2004; Lewis and Pollard, 2006). Our data suggest that TAMs are a very heterogeneous population; our technology enabled us to identify

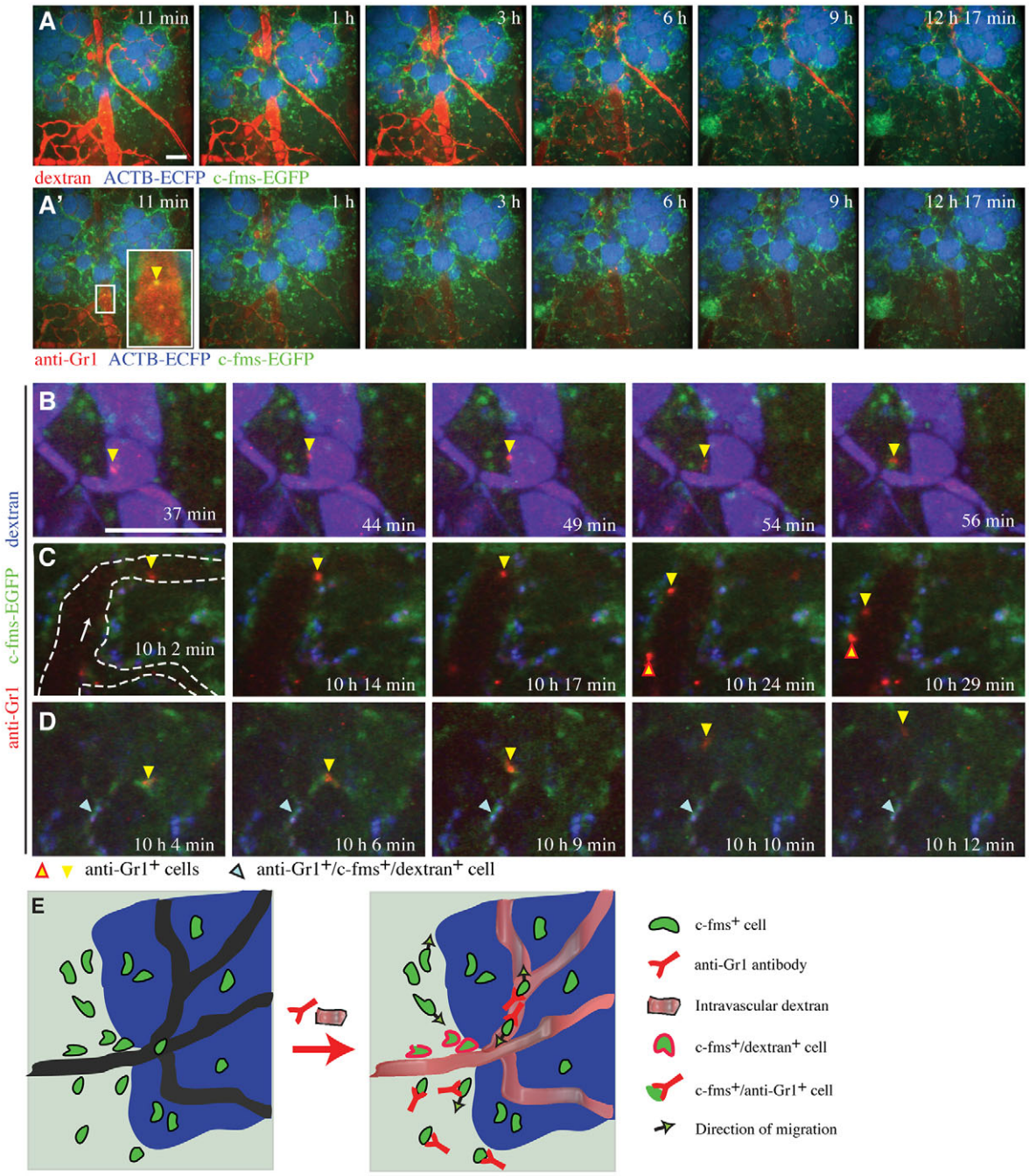

Fig. 6. Gr1$^+$ myeloid cells patrol tumor vessels, extravasate, and migrate in the tumor stroma. Four-color time-lapse series of the same lesion from an *MMTV-PyMT;ACTB-ECFP;c-fms-EGFP* mouse co-injected with fluorescent (A) 70 kDa dextran and (A') anti-Gr1 antibody. (See supplementary material Movie 9.) (B) A Gr1$^+$ cell (yellow arrowhead) extravasates from a dextran- (blue) and antibody-containing blood vessel (resulting in magenta). (C) c-fms$^+$/Gr1$^+$ (green/red) cells patrol the tumor vasculature. Two single cells going in opposite directions were tracked over time (yellow arrowhead, and yellow arrowhead with red outline). (D) A c-fms$^+$/Gr1$^+$ (green/red) cell migrates in the tumor stroma, next to a non-migratory, dextran-ingesting c-fms$^+$/Gr1$^+$ cell (cyan arrowhead). (E) Overview of combinatorial labeling techniques used with intravital micro-lensed spinning disk confocal imaging to achieve spatial, behavioral, functional, and molecular subdivision of c-fms$^+$ cells. Images are maximum intensity projections. Bars,100 μm

several populations of tumor-infiltrating myeloid cells with distinct behavioral and molecular characteristics. We used static markers on fixed tissue to correlate dextran ingestion, a marker of low migration, with markers of the alternatively activated macrophages. This enabled us to classify c-fms$^+$ myeloid cells into three distinct populations: motile CD68$^+$/CD206$^-$/dextran$^-$ cells in the peri-tumor areas; sessile CD68$^+$/CD206$^+$/dextran$^+$ alternatively activated macrophages in the peri-tumor areas; and sessile

CD68$^+$/CD206$^-$/dextran$^-$ cells within the tumor mass. Utilizing surface marker detection in vivo, we further classified the migratory c-fms$^+$ myeloid cells that did not ingest dextran into Gr1$^-$ and Gr1$^+$ populations. Based on our FACS data, the fast migratory c-fms$^+$/Gr1$^+$ cell population in the tumor stroma probably consists of granulocytes, MDSCs or monocytes (Geissmann et al., 2003). The c-fms$^+$/Gr1$^+$ cells that patrol blood vessels are probably monocytes, which have recently been described patrolling in the vasculature in areas of inflammation (Auffray et al., 2007). A few non-migratory dextran$^+$ cells were also weakly positive for the anti-Gr1 antibody, possibly representing cells that have differentiated from CD11b$^+$/Gr1$^+$ MDSCs, as these cells can be progenitors of TAMs (Sica and Bronte, 2007).

Dextran ingestion identified low-migratory c-fms$^+$ cells expressing CD206, a marker for alternatively activated M2 macrophages. M2 macrophages have poor antigen presenting capabilities, suppress T-cell activity and promote angiogenesis (Mantovani et al., 2002), and dextran ingestion marks macrophages that help cancer cells intravasate (Wyckoff et al., 2007). We found that the dextran-ingesting c-fms$^+$ cells express both CD68 and CD206. Since dextran is a ligand for CD206 (Sallusto et al., 1995), it is probable that receptor-mediated endocytosis is responsible for the association between dextran-uptake and CD206 expression. Interestingly, the sessile CD68$^+$ macrophages from within the tumor mass were distinct from those at the tumor-stroma border, as they did not take up dextran. Although dextran may not have penetrated into the tumor owing to high hydrostatic pressure, these macrophages also lacked CD206.

Imaging technology for long-term, multicolor imaging of cell behavior in tumor microenvironments in vivo

Multicolor intravital imaging techniques have been developed to study tumor-host interactions in real time (Yang et al., 2003; Hoffman, 2005; Yamauchi et al., 2005; Bouvet et al., 2006; Hoffman and Yang, 2006; Yang et al., 2007). However, it has been difficult to compare and contrast cell behavior in different tumor regions, and to image both acute (minutes) and long-term (>12 hours) cell behavior. We developed a novel combination of improved long-term anesthesia protocols, multi-region imaging, and combinatorial fluorescent labeling for imaging in live mice. We used these techniques with micro-lensed spinning disk confocal microscopy, but they can also be used individually or coordinately with other imaging modalities. Our techniques allowed us to compare cell dynamics between cell populations and microenvironments in the same mouse, with all systemic variables kept equal for >12 hours.

We designed our microscope to accommodate the standard transgenic mouse lines and imaging reagents, even when doing so required solving optical challenges. For example, imaging of ECFP and EGFP is non-trivial, but important, since EGFP and ECFP reporter mice are more common than red fluorescent reporter mice. Furthermore, many useful reporters are not very bright, necessitating high sensitivity imaging. We demonstrated this capability by imaging CD11c$^+$ cells, which express EGFP barely above the detection limit by FACS.

Our microscope system accommodates widely varied experimental designs from simple high-speed experiments (60 and 90 frames per second at resolutions of 512×512 and 240×240 pixels, respectively) to long-term, multi-position imaging in four colors and three dimensions over an entire day. Four lines of excitation give great flexibility in labeling techniques, demonstrated here by combining fluorescent proteins, fluorescent dextrans and FACS-validated antibodies. Other major advantages of our imaging system are the large image size (676×676 μm) at which we can acquire good resolution (0.66 μm/pixel), and the ability to image in well-lit rooms, aiding the monitoring of the mice.

Multi-photon microscopy can achieve deeper tissue penetration than spinning disk confocal microscopy (Wyckoff et al., 2007) and can image collagen through second harmonic generation (Brown et al., 2003). However, it is less flexible for multicolor excitation and requires imaging in darkness, making long-term monitoring of anesthetized mice more challenging. Thus, our imaging techniques complement other available approaches (Jain et al., 2002; Halin et al., 2005; Hoffman, 2005; Hoffman and Yang, 2006; Boissonnas et al., 2007; Wyckoff et al., 2007).

CONCLUSIONS AND PERSPECTIVES

Tumor biopsies have provided insights into the contribution of stromal cells for tumor progression, but cannot inform us about the dynamic behavior of these cells. To investigate the influence of the tumor microenvironment on cell behavior experimentally, we used the progressive *MMTV-PyMT* mouse model of cancer and observed cell behavior in different tumor regions. Moreover, we demonstrated the feasibility of directly manipulating the microenvironment in real time by changing oxygen levels. More sophisticated manipulations of microenvironmental factors should be possible in the future using genetic, transplantation and pharmacological approaches alone, or in combination.

The *MMTV-PyMT* model shares molecular and histological characteristics with human epidermal growth factor receptor 2 (HER2)-positive breast cancer (Lin et al., 2003; Herschkowitz et al., 2007). However, whether cells in human tumors behave similarly remains an open question, because no comparable data exist. Techniques are being developed for single-color endoscopic imaging in humans (Hoffman et al., 2006), but four-color, long-term tumor imaging is currently not feasible. Thus, establishing static markers of cellular behavior (such as dextran ingestion) will be necessary to confirm the human relevance of findings on cellular dynamics in mice.

We identified different behaviors of tumor-associated stromal cells in different tumor microenvironments, establishing the microenvironment as an experimental parameter that can be studied in real time, in live mice (supplementary material Movies 3,5,8). In addition, we subdivided the stromal c-fms$^+$ cell population into spatially, behaviorally and functionally distinct subpopulations. The tumor-promoting functions of two myeloid cell populations, the Gr1$^+$ cells and the macrophages, have been shown previously in experiments that have ablated Gr1$^+$ cells (Nozawa et al., 2006) or genetically restricted the numbers of monocytes/macrophages (Lin et al., 2001; Lin et al., 2006). However, these myeloid cell populations clearly display behavioral heterogeneity.

Our results have begun to address the challenge of separating out the functions and behaviors of the different tumor-associated host cell subpopulations, through the process of visualizing the tumor as a living tissue with multiple cellular components. Further experiments that combine pharmacological inhibition or genetic ablation with imaging technologies will complete the link of cell

behavior with function in tumor progression. The techniques are obviously not limited to the study of cancer, and will facilitate a new understanding of how cells function in their native microenvironments in development and disease.

METHODS

Mice and injections

Mice were crosses between the following strains: *MMTV-PyMT* and/or *ACTB-ECFP* (both from Jackson laboratory), and *Foxp3*^{EGFP}, *CD11c-DTR-EGFP*, *c-fms-EGFP*, *Fsp1*$^{+/+.EGFP}$ or *Sca1*$^{EGFP/+}$ (Guy et al., 1992; Hadjantonakis et al., 2002; Jung et al., 2002; Hanson et al., 2003; Sasmono et al., 2003; Xue et al., 2003; Fontenot et al., 2005). The numbers of mice used to study cell behavior were: six *MMTV-PyMT;ACTB-ECFP;Foxp3*^{EGFP}, three *MMTV-PyMT;ACTB-ECFP;CD11c-DTR-EGFP*, seven *MMTV-PyMT;ACTB-ECFP;c-fms-EGFP*, three *ACTB-ECFP;c-fms-EGFP* and two *MMTV-PyMT;ACTB-ECFP; Fsp1*$^{+/+.EGFP}$ mice. In addition, four *MMTV-PyMT;ACTB-ECFP;Foxp3*^{EGFP} mice and three *MMTV-PyMT;ACTB-ECFP;c-fms-EGFP* mice were used to study cellular responses to acute hypoxia. Two *MMTV-PyMT;ACTB-ECFP;c-fms-EGFP* mice were injected intravenously with 100 µl of sterile PBS containing 4 mg/ml of 70 kDa rhodamine-conjugated dextran (Invitrogen) and either 75 µg unlabeled and 25 µg Alexa Fluar 647-conjugated anti-Gr1 antibody (clone RB6-8C5, from the UCSF Hybridoma Core), or identical amounts of labeled and unlabeled isotype-matched control antibody. The tumor lesions were divided into broad categories that were recognizable in vivo: hyperplasias were defined as lesions with a diameter of less than 500 µm without excess stromal cell infiltration or invasion fronts; early carcinomas were small to medium lesions with increased stromal cell infiltration and invasion fronts; and late carcinomas were large lesions with compact cancer cells and massive stromal cell infiltration at the stromal border. All animal experiments were conducted in accordance with procedures approved by the Institutional Animal Care and Use Committee, UCSF.

Confocal imaging of live mice

Details of the microscope design and manufacturer information are listed in the supplementary material (Fig. S1). Briefly, a micro-lensed, spinning disk confocal scan-head was coupled to a motorized, inverted fluorescence microscope, and four-color imaging was achieved using argon and krypton lasers, a 405 nm solid-state laser, and selective emission filters. Images were collected using an ICCD camera (XR-Mega-10EX S-30, Stanford Photonics, Palo Alto, CA), with photon amplification of 20,000× prior to the CCD, whereas other cameras amplify the signal after the CCD. The CCD read-out noise (related to the pixel clock speed) does not limit the photon detection level. The combination of micro-lensed, spinning disk technology, with the ICCD camera technology facilitates the low light imaging that enables the long duration of experiments. For live, long-term, multi-position imaging using a robotic stage, an air lens was selected for ease of use. We obtained the best performance with a 10× Fluar, 0.5 NA lens, which was bright, resulted in negligible photobleaching when using fluorescent proteins, and could provide images from up to 70 µm into the tissue. Furthermore, it collected data from a large region (676 × 676 µm) at 0.66 µm/pixel.

Surgical procedures and anesthesia

Mice were initially anesthetized with 4% isoflurane (at 21% oxygen, balance nitrogen, Summit Anesthesia Solutions, OR), and surgery was performed with 2.5% isoflurane. The ventral surface of the mouse was prepared for surgery with isopropyl alcohol, a ventral midline incision was then made with sterilized scissors, the inguinal mammary fat pad was surgically exposed and a glass microscope slide was glued to the skin behind the mammary gland. The glass slide was rotated to expose the inner surface of the mammary gland, and the mouse was transferred to the microscopic stage. During imaging, isoflurane was reduced to the lowest concentration at which the mouse did not react to pain, typically 0.9-1.1%. We used an oximeter probe (MouseOx, Starr Life Sciences, PA) to monitor and display the heart rate (beats per minute; bpm), the arterial oxygen saturation of the blood (%), and the distension of blood vessels caused by the pulse and breathing (µm). This real-time feedback allowed us to adjust the anesthesia levels to the individual mouse. During the imaging procedure, isoflurane was delivered in a humidified mix of nitrogen and oxygen (at least 21%), with oxygen adjusted to achieve >95% oxygen saturation of arterial blood as measured with an oximeter probe. Mice received 50-100 µl/hour of saline intraperitonally and were covered with a recirculating heated water blanket during imaging (Gaymar, Orchard Park, NY). We have imaged 69 mice of various genotypes with a median time under anesthesia of 7 hours 29 minutes (range: 2 hours 45 minutes-27 hours 29 minutes).

Induction of acute systemic hypoxia

Acute systemic hypoxia was induced by lowering inhaled oxygen concentration to 7% for 20 minutes, followed by normalization with 21% oxygen. During imaging, mice received saline intraperitonally and were covered with a heated blanket.

Histology and immunostaining

Tissue sections (4% paraformaldehyde fixed, paraffin embedded, 5 µm sections) were stained with hematoxylin and eosin using standard methods. For labeling of leukocytes, frozen sections [methanol:acetone (1:1) fixed, 23 µm optical sections] were incubated with FITC-conjugated anti-CD45, or isotype control antibodies (BD Pharmingen) diluted 1:100, washed, and counter-stained with 1 µg/ml propidium iodide (Invitrogen). For labeling of CD68 and CD206, frozen sections from *MMTV-PyMT;ACTB-ECFP;c-fms-EGFP* tumors (harvested 4 hours after intravenous injection of 10 kDa Alexa Fluor 647-conjugated dextran, fixed in 4% paraformaldehyde) were incubated with anti-CD68, anti-CD206 antibody or isotype control antibody (Serotec) diluted 1:50, washed, and then incubated with secondary Alexa Fluor 568-conjugated anti-rat antibody (Invitrogen) diluted 1:150. Staining for CD68 and CD206 was conducted on five tumors from four mice.

FACS analysis of tumor infiltrating leukocytes

Mice were anesthetized with 2.5% avertin, and cardiac perfused with PBS at 110-120 mmHg until the flow-through fluid was clear. Tumors (diameter 8-12 mm) were isolated, chopped with razor blades, and digested with 2µg/ml collagenase type IV (Sigma C5138) in DME H-21 containing 5% fetal calf serum (FCS) and 5 µg/ml insulin for 30 minutes at 37°C, and then washed with DME H-21 with 5% FCS. The cells were resuspended in DME H-21

containing 5% FCS and 50 units/ml of DNAse (Sigma D4263), and the suspension slurry was run sequentially through 70 μm and 40 μm meshes. The resulting single cell suspensions were counted, and 5×10^5 cells were incubated with Fc-Block and then with fluorescently conjugated antibodies against cell-type specific markers (BD Biosciences and AbD Serotec) at 4°C for 30 minutes, the cells were then washed twice with PBS (without calcium or magnesium) with 1% FCS. The vital stain 7-ADD was added and the stained populations were analyzed using Becton-Dickinson FACScan and FlowJo software. For characterization of the different leukocyte populations, results from four *MMTV-PyMT* mice, analyzed separately, were averaged. For characterization of the cell populations that express c-fms-EGFP in tumors, cells from four *MMTV-PyMT;c-fms-EGFP* tumors were pooled and analyzed together.

Image analysis and cell tracking

All data sets were corrected for respiratory motion artifacts using Bitplane Imaris (version 5.5 or 5.7 for Windows X64) 'drift correction' with spot detection at a minimum diameter of 20 μm and Brownian movement algorithm with a maximum radius of 50 μm. Migration of Tregs and myeloid cells was analyzed using Bitplane Imaris (version 5.7 for Windows X64). Migration of Tregs was tracked manually using the measurement point function of Bitplane Imaris (version 5.7 for Windows X64). All cells present for five or more time points were tracked in six fields from three mice (n=130). Non-migration was defined as an average track length/time of <1 μm/minute and a total displacement over the entire observation period of <10 μm. Cells were considered to have arrested when they stayed within a 10 μm radius for 5 minutes or longer. The distance of migratory Tregs from blood vessels was estimated on 13 fields from 5 mice (n=98) and the median and range of these estimations are reported. Tracking of Tregs before, during, and after acute hypoxia was carried out using ImageJ 1.34 software. Owing to the large number of myeloid cells, their migration was analyzed automatically using Bitplane Imaris with spot detection at a minimum diameter of 8 μm and Brownian movement algorithm with a maximum radius of 14 μm/minute, in 1 hour image sets, with 40-48 seconds between frames, in 200 × 200 μm fields, which more accurately covered one microenvironment than the entire image fields. Velocity, defined as the magnitude of the average velocity vector, was calculated as the ratio between total displacement and total time tracked, and reported for all tracks with duration of at least five time points. For each tissue microenvironment, four or more different fields in at least three different mice were analyzed. For tracking of myeloid cells before, during, and after induction of acute systemic hypoxia, the entire image field was tracked. Cell tracking is intrinsically difficult in live tissues because cells change intensity or diameter as they squeeze through the tissue, and because of limited contrast between individual cells in areas with high cell infiltration. Displacement is, therefore, a more robust measure, and better for comparing single cell migration between mice than track length. Displacement is not sensitive to the time intervals between image acquisition, whereas motion artifacts lead to overestimation of track length with a large mouse-to-mouse variation (Shakhar et al., 2005). However, since cells rarely migrate in straight lines, migratory displacement is shorter than the path length, and the magnitude of the average velocity vector, which we used to compare migration, is much smaller than the maximal instantaneous speed the myeloid cells can achieve in vivo. These challenges are not intrinsic to our technique.

TRANSLATIONAL IMPACT

Clinical issue

White blood cells are attracted to sites of infection or tumors to defend the organism. However, instead of attacking tumors, some white blood cells stimulate tumor growth and cancer spreading. Knowledge of how these cells behave in tumors could contribute to the understanding of how the cells promote cancer, but little is known about their real-time behavior.

Results

In this paper, a system is described that monitors white blood cells inside tumors of live mice for up to 12 hours. This system is built around a spinning disk confocal microscope. It uses genetically engineered mice that model the aggressive HER2-expressing human breast cancer, where the cancer cells and white blood cells have been given different fluorescent colors.

The white blood cells moved differently depending on their position in the tumor. At the tumor periphery, one cell population moved, whereas another did not. A third population, which had penetrated into the tumor, was also motionless. Since oxygen levels are lower inside tumors than at the periphery, it was tested whether moving cells would slow down when the mice were ventilated with reduced oxygen concentrations. The myeloid cells originating from the bone marrow remained unaffected. In contrast, regulatory T-lymphocytes, originating from the lymph nodes, stopped migrating when the oxygen concentration was lowered. This finding suggests that the low oxygen levels in tumors reduce the ability of some white blood cells to penetrate into the tumor, while leaving others unaffected.

To mark the blood vessels, a fluorescently labeled polysaccharide, dextran, was injected, which leaked out of the blood vessels and was ingested by stationary, alternatively activated macrophages, a myeloid cell type that promotes tumor progression. In contrast, $Gr1^+$ myeloid cells moved, both inside tumor blood vessels and at the tumor periphery. Therefore, these two myeloid-derived cell populations behaved distinctly.

Implications and future directions

An immediate application of the live microscopy system described here is to watch cancer drugs in action. Development of live microscopy in humans or, of human tissue samples, is necessary to confirm the human relevance. Insights into the behavior of white blood cells in tumors could help solve why some of these cells promote tumor growth. This could lead to new ideas on how to treat cancer. The techniques are not limited to the study of cancer, but could help gain new understanding of how cells function in live organs, healthy or diseased.

doi:10.1242/dmm.001081

Statistical methods

The distributions of myeloid cells into slow, medium and fast migratory cells in different microenvironments were analyzed by chi-square test using the total number of cells in each category. GraphPad Prism 4 software and alpha=0.05 were used.

ACKNOWLEDGEMENTS

We thank Drs David Hume, Jeffrey Pollard, Timothy Graubert, Alexander Rudensky, Qizhi Tang and Eric Neilson for mice; Dr Susan Watson, Elena Atamaniuc and Ying Yu for technical support; and John Zemek and Dr Gary Rondeau for help in customizing the microscope stage and filter wheel. This work was supported by NIH grants (AI053194, CA057621, CA105379, ES012801 and RR019401), a grant from the Cancer Research Institute (M.F.K.) and fellowships from The Danish Medical Research Council (M.E.), an NIH NRSA (HL-007731), and the California Breast Cancer Research Program (11FB-0015) (A.J.E.). H.A.A. was supported by the

Research Council of Norway (Functional Genomics Program [151882] and project support 160698/V40).

COMPETING INTERESTS

G.P. has a personal financial interest in Solamere Technology Group that custom builds microscopes similar to the one presented in the manuscript and therefore declares competing financial interest.

AUTHOR CONTRIBUTIONS

M.E. and A.J.E. contributed equally to this study. M.E., A.J.E., B.E.W. and Z.W. conceived the imaging strategies; A.J.E. and G.P. designed and built the spinning disk confocal microscope with contributions from M.E. and Z.W.; M.E. and Z.W. designed the experiments with contributions from A.J.E. and M.F.K.; M.E, H.A.A. and E.B. did the live imaging experiments; M.E and H.A.A. did analysis of live imaging experiments with contributions from A.J.E.; M.E., H.A.A. and A.J.E. did immunostainings; M.L.T. did the FACS experiments and the analysis; M.E., A.J.E. and Z.W. wrote the manuscript.

SUPPLEMENTARY MATERIAL

Supplementary material for this article is available at
http://dmm.biologists.org/content/1/2-3/155/suppl/DC1

Received 15 April 2008; Accepted 18 June 2008.

REFERENCES

Auffray, C., Fogg, D., Garfa, M., Elain, G., Join-Lambert, O., Kayal, S., Sarnacki, S., Cumano, A., Lauvau, G. and Geissmann, F. (2007). Monitoring of blood vessels and tissues by a population of monocytes with patrolling behavior. *Science* **317**, 666-670.

Banchereau, J. and Palucka, A. K. (2005). Dendritic cells as therapeutic vaccines against cancer. *Nat. Rev. Immunol.* **5**, 296-306.

Bhowmick, N. A. and Moses, H. L. (2005). Tumor-stroma interactions. *Curr. Opin. Genet. Dev.* **15**, 97-101.

Bissell, M. J. and Radisky, D. (2001). Putting tumours in context. *Nat. Rev. Cancer* **1**, 46-54.

Boissonnas, A., Fetler, L., Zeelenberg, I. S., Hugues, S. and Amigorena, S. (2007). In vivo imaging of cytotoxic T cell infiltration and elimination of a solid tumor. *J. Exp. Med.* **204**, 345-356.

Bouvet, M., Tsuji, K., Yang, M., Jiang, P., Moossa, A. R. and Hoffman, R. M. (2006). In vivo color-coded imaging of the interaction of colon cancer cells and splenocytes in the formation of liver metastases. *Cancer Res.* **66**, 11293-11297.

Brown, E., McKee, T., diTomaso, E., Pluen, A., Seed, B., Boucher, Y. and Jain, R. K. (2003). Dynamic imaging of collagen and its modulation in tumors in vivo using second-harmonic generation. *Nat. Med.* **9**, 796-800.

Brown, E. B., Campbell, R. B., Tsuzuki, Y., Xu, L., Carmeliet, P., Fukumura, D. and Jain, R. K. (2001). In vivo measurement of gene expression, angiogenesis and physiological function in tumors using multiphoton laser scanning microscopy. *Nat. Med.* **7**, 864-868.

Brown, J. M. and Wilson, W. R. (2004). Exploiting tumour hypoxia in cancer treatment. *Nat. Rev. Cancer* **4**, 437-447.

Chiang, E. Y., Hidalgo, A., Chang, J. and Frenette, P. S. (2007). Imaging receptor microdomains on leukocyte subsets in live mice. *Nat. Methods* **4**, 219-222.

Colombo, M. P. and Piconese, S. (2007). Regulatory-T-cell inhibition versus depletion: the right choice in cancer immunotherapy. *Nat. Rev. Cancer* **7**, 880-887.

Condeelis, J. and Pollard, J. W. (2006). Macrophages: obligate partners for tumor cell migration, invasion, and metastasis. *Cell* **124**, 263-266.

Coussens, L. M. and Werb, Z. (2002). Inflammation and cancer. *Nature* **420**, 860-867.

de Visser, K. E., Eichten, A. and Coussens, L. M. (2006). Paradoxical roles of the immune system during cancer development. *Nat. Rev. Cancer* **6**, 24-37.

Dreher, M. R., Liu, W., Michelich, C. R., Dewhirst, M. W., Yuan, F. and Chilkoti, A. (2006). Tumor vascular permeability, accumulation, and penetration of macromolecular drug carriers. *J. Natl. Cancer Inst.* **98**, 335-344.

Du, R., Lu, K. V., Petritsch, C., Liu, P., Ganss, R., Passegue, E., Song, H., Vandenberg, S., Johnson, R. S., Werb, Z. et al. (2008). HIF1alpha induces the recruitment of bone marrow-derived vascular modulatory cells to regulate tumor angiogenesis and invasion. *Cancer Cell* **13**, 206-220.

Egeblad, M. and Werb, Z. (2002). New functions for the matrix metalloproteinases in cancer progression. *Nat. Rev. Cancer* **2**, 161-174.

Fontenot, J. D., Rasmussen, J. P., Williams, L. M., Dooley, J. L., Farr, A. G. and Rudensky, A. Y. (2005). Regulatory T cell lineage specification by the forkhead transcription factor foxp3. *Immunity* **22**, 329-341.

Gabrilovich, D. I., Bronte, V., Chen, S. H., Colombo, M. P., Ochoa, A., Ostrand-Rosenberg, S. and Schreiber, H. (2007). The terminology issue for myeloid-derived suppressor cells. *Cancer Res.* **67**, 425; author reply 426.

Geissmann, F., Jung, S. and Littman, D. R. (2003). Blood monocytes consist of two principal subsets with distinct migratory properties. *Immunity* **19**, 71-82.

Gray, J. M., Karow, D. S., Lu, H., Chang, A. J., Chang, J. S., Ellis, R. E., Marletta, M. A. and Bargmann, C. I. (2004). Oxygen sensation and social feeding mediated by a C. elegans guanylate cyclase homologue. *Nature* **430**, 317-322.

Grimshaw, M. J. and Balkwill, F. R. (2001). Inhibition of monocyte and macrophage chemotaxis by hypoxia and inflammation-a potential mechanism. *Eur. J. Immunol.* **31**, 480-489.

Grundy, M. and Sentman, C. L. (2005). GFP transgenic mice show dynamics of lung macrophages. *Exp. Cell Res.* **310**, 409-416.

Guy, C. T., Cardiff, R. D. and Muller, W. J. (1992). Induction of mammary tumors by expression of polyomavirus middle T oncogene: a transgenic mouse model for metastatic disease. *Mol. Cell. Biol.* **12**, 954-961.

Hadjantonakis, A. K., Macmaster, S. and Nagy, A. (2002). Embryonic stem cells and mice expressing different GFP variants for multiple non-invasive reporter usage within a single animal. *BMC Biotechnol.* **2**, 11.

Halin, C., Rodrigo Mora, J., Sumen, C. and von Andrian, U. H. (2005). In vivo imaging of lymphocyte trafficking. *Annu. Rev. Cell Dev. Biol.* **21**, 581-603.

Hanson, P., Mathews, V., Marrus, S. H. and Graubert, T. A. (2003). Enhanced green fluorescent protein targeted to the Sca-1 (Ly-6A) locus in transgenic mice results in efficient marking of hematopoietic stem cells in vivo. *Exp. Hematol.* **31**, 159-167.

Herschkowitz, J. I., Simin, K., Weigman, V. J., Mikaelian, I., Usary, J., Hu, Z., Rasmussen, K. E., Jones, L. P., Assefnia, S., Chandrasekharan, S. et al. (2007). Identification of conserved gene expression features between murine mammary carcinoma models and human breast tumors. *Genome Biol.* 8, R76.

Hoffman, A., Goetz, M., Vieth, M., Galle, P. R., Neurath, M. F. and Kiesslich, R. (2006). Confocal laser endomicroscopy: technical status and current indications. *Endoscopy* **38**, 1275-1283.

Hoffman, R. M. (2005). The multiple uses of fluorescent proteins to visualize cancer in vivo. *Nat. Rev. Cancer* **5**, 796-806.

Hoffman, R. M. and Yang, M. (2006). Color-coded fluorescence imaging of tumor-host interactions. *Nat. Protoc.* **1**, 928-935.

Huang, J. H., Cardenas-Navia, L. I., Caldwell, C. C., Plumb, T. J., Radu, C. G., Rocha, P. N., Wilder, T., Bromberg, J. S., Cronstein, B. N., Sitkovsky, M. et al. (2007). Requirements for T lymphocyte migration in explanted lymph nodes. *J. Immunol.* **178**, 7747-7755.

Inoue, T., Plieth, D., Venkov, C. D., Xu, C. and Neilson, E. G. (2005). Antibodies against macrophages that overlap in specificity with fibroblasts. *Kidney Int.* **67**, 2488-2493.

Jain, R. K., Munn, L. L. and Fukumura, D. (2002). Dissecting tumour pathophysiology using intravital microscopy. *Nat. Rev. Cancer* **2**, 266-276.

Jung, S., Unutmaz, D., Wong, P., Sano, G., De los Santos, K., Sparwasser, T., Wu, S., Vuthoori, S., Ko, K., Zavala, F. et al. (2002). In vivo depletion of CD11c(+) dendritic cells abrogates priming of CD8(+) T cells by exogenous cell-associated antigens. *Immunity* **17**, 211-220.

Labeur, M. S., Roters, B., Pers, B., Mehling, A., Luger, T. A., Schwarz, T. and Grabbe, S. (1999). Generation of tumor immunity by bone marrow-derived dendritic cells correlates with dendritic cell maturation stage. *J. Immunol.* **162**, 168-175.

Lewis, C. E. and Pollard, J. W. (2006). Distinct role of macrophages in different tumor microenvironments. *Cancer Res.* **66**, 605-612.

Lin, E. Y., Nguyen, A. V., Russell, R. G. and Pollard, J. W. (2001). Colony-stimulating factor 1 promotes progression of mammary tumors to malignancy. *J. Exp. Med.* **193**, 727-740.

Lin, E. Y., Jones, J. G., Li, P., Zhu, L., Whitney, K. D., Muller, W. J. and Pollard, J. W. (2003). Progression to malignancy in the polyoma middle T oncoprotein mouse breast cancer model provides a reliable model for human diseases. *Am. J. Pathol.* **163**, 2113-2126.

Lin, E. Y., Li, J. F., Gnatovskiy, L., Deng, Y., Zhu, L., Grzesik, D. A., Qian, H., Xue, X. N. and Pollard, J. W. (2006). Macrophages regulate the angiogenic switch in a mouse model of breast cancer. *Cancer Res.* **66**, 11238-11246.

Lindquist, R. L., Shakhar, G., Dudziak, D., Wardemann, H., Eisenreich, T., Dustin, M. L. and Nussenzweig, M. C. (2004). Visualizing dendritic cell networks in vivo. *Nat. Immunol.* **5**, 1243-1250.

Mantovani, A., Sozzani, S., Locati, M., Allavena, P. and Sica, A. (2002). Macrophage polarization: tumor-associated macrophages as a paradigm for polarized M2 mononuclear phagocytes. *Trends Immunol.* **23**, 549-555.

Mordue, D. G. and Sibley, L. D. (2003). A novel population of Gr-1+-activated macrophages induced during acute toxoplasmosis. *J. Leukoc. Biol.* **74**, 1015-1025.

Mrass, P., Takano, H., Ng, L. G., Daxini, S., Lasaro, M. O., Iparraguirre, A., Cavanagh, L. L., von Andrian, U. H., Ertl, H. C., Haydon, P. G. et al. (2006). Random migration precedes stable target cell interactions of tumor-infiltrating T cells. *J. Exp. Med.* **203**, 2749-2761.

Murdoch, C., Giannoudis, A. and Lewis, C. E. (2004). Mechanisms regulating the recruitment of macrophages into hypoxic areas of tumors and other ischemic tissues. *Blood* **104**, 2224-2234.

Nozawa, H., Chiu, C. and Hanahan, D. (2006). Infiltrating neutrophils mediate the initial angiogenic switch in a mouse model of multistage carcinogenesis. *Proc. Natl. Acad. Sci. USA* **103**, 12493-12498.

Pollard, J. W. (2004). Tumour-educated macrophages promote tumour progression and metastasis. *Nat. Rev. Cancer* **4**, 71-78.

Sallusto, F., Cella, M., Danieli, C. and Lanzavecchia, A. (1995). Dendritic cells use macropinocytosis and the mannose receptor to concentrate macromolecules in the major histocompatibility complex class II compartment: downregulation by cytokines and bacterial products. *J. Exp. Med.* **182**, 389-400.

Sasmono, R. T., Oceandy, D., Pollard, J. W., Tong, W., Pavli, P., Wainwright, B. J., Ostrowski, M. C., Himes, S. R. and Hume, D. A. (2003). A macrophage colony-stimulating factor receptor-green fluorescent protein transgene is expressed throughout the mononuclear phagocyte system of the mouse. *Blood* **101**, 1155-1163.

Shakhar, G., Lindquist, R. L., Skokos, D., Dudziak, D., Huang, J. H., Nussenzweig, M. C. and Dustin, M. L. (2005). Stable T cell-dendritic cell interactions precede the development of both tolerance and immunity in vivo. *Nat. Immunol.* **6**, 707-714.

Sica, A. and Bronte, V. (2007). Altered macrophage differentiation and immune dysfunction in tumor development. *J. Clin. Invest.* **117**, 1155-1166.

Sidani, M., Wyckoff, J., Xue, C., Segall, J. E. and Condeelis, J. (2006). Probing the microenvironment of mammary tumors using multiphoton microscopy. *J. Mammary Gland Biol. Neoplasia* **11**, 151-163.

Stroh, M., Zimmer, J. P., Duda, D. G., Levchenko, T. S., Cohen, K. S., Brown, E. B., Scadden, D. T., Torchilin, V. P., Bawendi, M. G., Fukumura, D. et al. (2005). Quantum dots spectrally distinguish multiple species within the tumor milieu in vivo. *Nat. Med.* **11**, 678-682.

Turner, L., Scotton, C., Negus, R. and Balkwill, F. (1999). Hypoxia inhibits macrophage migration. *Eur. J. Immunol.* **29**, 2280-2287.

Wyckoff, J. B., Wang, Y., Lin, E. Y., Li, J. F., Goswami, S., Stanley, E. R., Segall, J. E., Pollard, J. W. and Condeelis, J. (2007). Direct visualization of macrophage-assisted tumor cell intravasation in mammary tumors. *Cancer Res.* **67**, 2649-2656.

Xue, C., Plieth, D., Venkov, C., Xu, C. and Neilson, E. G. (2003). The gatekeeper effect of epithelial-mesenchymal transition regulates the frequency of breast cancer metastasis. *Cancer Res.* **63**, 3386-3394.

Yamauchi, K., Yang, M., Jiang, P., Yamamoto, N., Xu, M., Amoh, Y., Tsuji, K., Bouvet, M., Tsuchiya, H., Tomita, K. et al. (2005). Real-time in vivo dual-color imaging of intracapillary cancer cell and nucleus deformation and migration. *Cancer Res.* **65**, 4246-4252.

Yang, M., Li, L., Jiang, P., Moossa, A. R., Penman, S. and Hoffman, R. M. (2003). Dual-color fluorescence imaging distinguishes tumor cells from induced host angiogenic vessels and stromal cells. *Proc. Natl. Acad. Sci. USA* **100**, 14259-14262.

Yang, M., Jiang, P. and Hoffman, R. M. (2007). Whole-body subcellular multicolor imaging of tumor-host interaction and drug response in real time. *Cancer Res.* **67**, 5195-5200.